Near-infrared color properties of Kuiper Belt Objects and Centaurs: Final results from the ESO Large Program*

*Based on observations collected at the European Southern Observatory, Chile, under program 167.C-0340.

Audrey Delsanti[1]

Institute for Astronomy and NASA Astrobiology Institute, 2680 Woodlawn Drive, Honolulu, Hawaii 96822, USA

delsanti@ifa.hawaii.edu

and

Nuno Peixinho[1]

CAAUL, Observatorio Astronomico de Lisboa, Tapada da Ajuda, PT-1349-018 Lisboa, Portugal

peixinho@oal.ul.pt

and

Hermann Boehnhardt

MPI, Max-Planck-Institute for Solar System Research, Max-Planck-Str. 2, D-37191 Katlenburg-Lindau, Germany

boehnhardt@linmpi.mpg.de

and

Maria-Antonietta Barucci and Frédéric Merlin and Alain Doressoundiram

LESIA, Observatoire de Paris-Meudon, 5 Place Jules Janssen, 92195 Meudon, France

Antonella.Barucci@obspm.fr, Frederic.Merlin@obspm.fr,

Alain.Doressoundiram@obspm.fr

and

John K. Davies

Astronomy Technology Centre, Royal Observatory, Blackford Hill, Edinburgh, EH9 3HJ, United Kingdom

jkd@roe.ac.uk

Received _____; accepted _____

[1]LESIA, Observatoire de Paris-Meudon, 5 Place Jules Janssen, 92195 Meudon, France

ABSTRACT

We present near-IR JHK broadband photometry for 17 Kuiper Belt Objects (KBOs) and Centaurs. The observations were performed within the ESO Large Program on the "Physical Properties of Kuiper Belt Object and Centaurs" from January 2001 to August 2002. We used the ISAAC instrument at the ESO 8m-Very Large Telescope. We compiled visible / near-IR colors for a total of 51 published objects and performed a statistical analysis. Color-color correlations show that a same coloring process is probably acting on Centaurs and KBOs surfaces from the visible to the near-IR range.

Centaurs with a $H-K$ smaller than the Sun (0.06) systematically display the reddest $B-V$ colors (at the 2.5σ level). These Centaur surfaces are suspected to harbor material that signs around 1.7–2.2μm (water ice is a possibility, it was reported for the three objects that have published spectroscopy). We report no statistically significant evidence for a bimodal structure of the VJHK Centaur colors (Kolmogorov-Smirnoff and dip tests on up to 17 objects). The Centaurs $H-K$ colors show some robust evidence (significance level SL >99.99%) for a continuous structure. We also report a statistically significant bimodal structure of the Centaur $B-R$ distribution, which is compatible with the results published in Peixinho et al. (2003) with different data.

Classical KBOs show no 3σ level trend. $V-J$ color is marginally correlated with perihelion distance q (which is consistent with results reported by Doressoundiram et al. 2005b, on $B-R$ colors). Resonant and scattered disk objects are under represented (7 and 9 objects resp.) and show no statistically significant trend. Some of the marginal trends are mentioned for subsequent monitoring.

Subject headings: Kuiper Belt – infrared: solar system – techniques: photometric –

methods: statistical

1. Introduction

The region of the Solar System beyond Neptune is populated by icy minor bodies known as trans-neptunians objects (TNOs) or Kuiper belt objects (KBOs). Since the discovery of 1992 QB_1 (Jewitt & Luu 1993), more than 1000 such objects have been detected. Due to their large heliocentric distances, KBOs are suspected to retain the most pristine material of the Solar System. From a dynamical point of view, KBOs are classified as: the classical objects (with circular orbits of moderate eccentricities), the resonant objects, trapped in mean motion resonances with Neptune (the 3:2 resonance hosts the "Plutinos", named after the largest of them, Pluto), and the scattered disk objects (SDOs). SDOs are believed to have had gravitational interactions with the giant planets at some point of their history, that caused their orbits to be eccentric and sometimes very inclined. Two extreme objects have been classified as "extended scattered disk" objects (Gladman et al. 2002); their perihelion is far outside the orbit of Neptune. Due to their faintness, KBOs are very difficult to study; their physical properties are far from being fully studied and understood (see summary by Barucci et al. 2004). Basic parameters such as size and albedo are known for a few objects and are difficult to measure. Physical information about KBOs comes from surface colors measurements through broadband filter, in the visible and near-IR range. Photometry provides only a general insight into KBOs physical properties. Surface composition is determined by reflectance spectroscopy. However, even with the use of 8-10m class telescopes, only the brightest KBOs can be studied (m_V ∼17–20). For a review on the current state of knowledge of the Kuiper Belt, please refer to the special issue of the Comptes rendus de l'Académie des Sciences "New frontiers in the Solar System: the Trans-Neptunian objects" (Fasicule 7, Sept. 2003, Ed. M.A. Barucci), or to "The First Decadal Review of the Edgeworth Kuiper Belt" (Earth Moon and Planets, Vol. 92, 2003).

The optical color diversity seems to prevail among the observed KBOs and Centaurs.

This diversity seems also to extend to near infrared wavelengths, although relatively few visible-NIR color datasets are available (see Delsanti et al. 2004; McBride et al. 2003, and references therein). Statistical analyses point to correlations between optical colors and some orbital parameters (i, e, q) for the classical objects (e.g. Hainaut & Delsanti 2002; Trujillo & Brown 2002; Doressoundiram et al. 2002; Peixinho et al. 2004). In contrast, no similar trends are obvious for Plutinos, SDOs or Centaurs. Another important result is the absence of correlation of colors with size or heliocentric distance for any of these populations. Here, we investigate if such similar trends exist for near-IR colors. Centaur visible colors display a bimodal structure that is statistically significant for $B - R$ index (Peixinho et al. 2003). This bimodal structure is difficult to understand from a physical point of view, and to date, no model has succeeded in reproducing the observed Centaur color distributions. In this paper, we present JHK colors for 17 Centaurs and KBOs. We then merge this sample with existing data to analyze a dataset of 51 objects with different statistical tools.

2. The ESO Large Program

This program was designed in the early 2000's under the leadership of H. Boehnhardt. At this time, visible surface colors were known for only a few objects (see for instance: Luu & Jewitt 1996; Green et al. 1997; Jewitt & Luu 1998; Barucci et al. 1999) and near-IR (mostly J) colors for an even smaller subset of KBOs (Green et al. 1997; Weintraub et al. 1997; Davies et al. 1998; McBride et al. 1999). A few spectra were published (Brown & Koresko 1998; Brown et al. 1999; Barucci et al. 1999). The goal of the ESO Large Program was to provide observational constraints to characterize the physical properties of a relatively large number of KBOs and Centaurs, using the collecting power of the four 8m-Very Large Telescopes at Cerro Paranal Observatory, Chile. The program started in 2001 and

encompassed photometric and spectroscopic measurements at visible and near-infrared wavelengths for a total of a hundred objects. The same instrumental set-up was used during the whole program (∼300h spread over 2 years) to ensure a good homogeneity of the dataset. The results of this program are presented in Boehnhardt et al. (2002); Peixinho et al. (2004), and this paper for the photometry and Barucci et al. (2002); Dotto et al. (2003); Doressoundiram et al. (2003); Lazzarin et al. (2003); Fornasier et al. (2004); Doressoundiram et al. (2005a) for spectroscopy.

3. Observations

The near-IR photometry observations were carried out at the ESO 8m-Very Large Telescope (VLT), Unit 1. We used the ISAAC (Infrared Spectrometer And Array Camera) instrument (installed at the Nasmyth B focus) in the short wavelength (SW) imaging mode. The SW arm is equipped with a 1024×1024 Hawaii Rockwell array with 18.5×18.5 micron/pixels. The pixel scale is 0.148 arcsec/pixel and the field of view is 2.5'×2.5'. We used the J, H and K_S filters, which have a central wavelength of 1.25, 1.65 and 2.16μm resp. and a width of $\sim 0.3\mu$m.

[**Table 1**]

The object list and the geometrical circumstances of the observations are summarized in Table 1. Some of the observations were executed in service mode over a period from April 2001 to January 2002, when the observational constraints (*e.g.* seeing better than 0.8" and a photometric or clear weather) were fulfilled. Observations from August 2002 were carried out in visitor mode. In both cases, imaging was done using a standard jittering method, dithering the telescope within 10" in between two sub-exposures according to a random pattern. The telescope tracked at sidereal rate. KBO apparent velocities are below

4" per hour and the typical image seeing is 0.65". Thus, there is no trailing of the KBOs with respect to the stars on a single sub-exposure (lower than a minute in all filters).

4. Data reduction and photometry

We corrected all frames from the "electrical ghost" effect before dark subtraction. We then applied a flat-field correction. Sky correction was performed using IRAF/xdimsum, a package optimized for background dominated data. The complete method is described in Delsanti et al. (2004). We recombined the individual sky-subtracted frames following two methods. We first stacked the images using multiple star centroids to get point-like stars. This composite was used for PSF estimation. In a second version, we take into account the KBO velocity (obtained from the JPL ephemeris) to stack the images. This composite (with a point-like KBO) was used for KBO photometry measurements.

We used standard stars (LCO/Palomar NICMOS Catalog, Persson et al. 1998) to estimate the zero-point of the instrument in the different filters. We used Paranal observatory typical extinction values provided by the ESO calibration plan, which are k_J=0.11, k_H=0.06, and k_K=0.07 mag/airmass. We neglected the instrument color transformation, as they lie below 1% for our solar system objects.

[**Table 2**]

We used an aperture correction method to measure the KBOs flux, as fully described in Delsanti et al. (2004). The sky background was estimated using five square apertures (of 25 pixels, *i.e.* 3.7" size) surrounding the object. We constructed a curve of growth for several non-saturated nearby stars in order to compute the aperture correction. The KBO magnitudes obtained using this method are listed in Table 2. UT times are given at mid-exposures. The error estimation on magnitudes ranges from 3 to 12% depending on

the objects. They include: error from the photometric calibration (systematic, a few %), error on the flux measurement (around 1–2%, contains the photon/instrumental noises) and error from the aperture correction (typically from 1–2 up to 8% depending on the quality and number of nearby stars found to build the curves of growth).

[**Table 3**]

Table 3 shows the solar colors, JHK colors for 17 objects from this paper (9 of them are published for the first time), and a summary of the ESO Large Program JHK photometry obtained within the spectroscopy part of the program. When multiple magnitudes of a given filter are available, color indexes are computed from the magnitudes the closest in time.

5. Results

5.1. Dynamical classification of the objects

There is currently no dynamical classification universally accepted by the community for the objects we are dealing with. The Minor Planet Center provides on a daily basis two different lists of orbital parameters: one for the "Transneptunian objects" (`http://cfa-www.harvard.edu/iau/lists/TNOs.html`) and one for the "Centaurs and Scattered disk objects" (`http://cfa-www.harvard.edu/iau/lists/Centaurs.html`) with no further distinction between the different sub-groups commonly quoted: classical objects, resonant objects, scattered disk objects, extended scattered disk objects and Centaurs.

For our color analysis, we adopt the same dynamical classification than in Doressoundiram et al. (2005b). The dynamical type of the objects is set as follows: 1) resonant objects are from Chiang et al. (2003), 2) classical objects are the objects from the Minor Planet Center "Trans-neptunian objects" list with a semimajor axis $39.5 < a < 48$

AU (*i.e.* between the 3:2 and 2:1 resonances), and perihelion $q > 35$ AU (*i.e.* outside Neptune's Hill sphere). Objects with $q > 36$ AU and $36 < a < 40$ AU with low inclination orbits are also stable and labeled as classical (Duncan et al. 1995). 3) Centaurs are the objects from the Minor Planet Center list "Centaurs and scattered disk objects" with perihelia smaller than Neptune's semimajor axis (30 AU) and aphelia $Q < 48$ AU (2:1 resonance); 4) SDOs are the objects left over from the sorting processes 2) and 3). The resulting classification for our sample is listed in Table 4.

5.2. The visible/near-IR color database

[**Table 4**]

We compiled the near-infrared colors published in the literature to work on a larger sample for the use of statistical tools. This color compilation is made in the framework of the MBOSS (Minor Bodies of the Outer Solar System) database project first published in Hainaut & Delsanti (2002), and regularly updated. The current database is available online: `http://www.sc.eso.org/~ohainaut/MBOSS/`. Table 4 contains the VJHK colors available for 51 objects. We also compiled previously published Bessell filter system BRI colors (for the sake of clarity, they do not appear in the table). **Note to the editor: do they need to appear somewhere (electronic table ?)**. We used and compiled the 1σ errors published by the different authors. In the final average color index of a given object, each observer contribution is weighted by $1/\sigma$, thus giving more weight to higher quality measurements. The error propagation is detailed in Hainaut & Delsanti (2002) p. 646.

[**Figure 1**]

The resulting $J - H$ vs $H - K$ plot in shown in Fig. 1–a. A close up on Centaur colors is shown on Fig. 1–b. The star symbol shows the solar colors. The "reddening

curve" drawn on the plot is described in Delsanti et al. (2004): it is the locus of objects with a reflectivity spectrum of increasing linear slope. The sun, as a reference, has a linear reflectivity spectrum with a null slope. A tick mark is placed every 10 %/100nm, the curve is graduated in units of spectral slope from 0 (solar) to 70%/100nm (very red). Most of the points lie below the reddening curve. This is an indication for a change and decrease of the spectral slope over the JHK range. Two outliers can be noticed: (19308) 1996 TO_{66} (point top-left) and (24835) 1995 SM_{55} (point bottom-left). (19308) 1996 TO_{66} was measured by Jewitt & Luu (1998) and Davies et al. (2000). This blue object was reported to have a non-repeatable visible light-curve over time (Hainaut et al. 2000; Sekiguchi et al. 2002) in amplitude, shape and rotation period. Sheppard & Jewitt (2003) later showed that only the light-curve amplitude might be varying. This result is confirmed by Belskaya et al. (ACM 2005, abstract P6.2). They match the amplitude increases with opposition surge effects that occur at small phase angles. Belskaya et al. also argue that phase angle effects are most probably responsible for the problems in determining an unambiguous rotation period. Object (24835) 1995 SM_{55} was measured by McBride et al. (2003) and Delsanti et al. (2004). The latter published a noticeably blue reflectivity spectrum (especially in the near-IR), which might be an indication for the presence –for example– of water ice (broad absorption band around 2μm). Unfortunately, this target is too faint to be observed in near-IR spectroscopy. According to Sheppard & Jewitt (2003), 1995 SM_{55} has a non-repeatable visible light-curve over time. Several causes are suggested: the presence of an unresolved companion, cometary activity, or –less likely– a complex rotational state.

6. Discussion

6.1. Color-color correlations

[**Table 5**]

[**Table 6**]

In this section we compare the different color samples (BVRIJHK and visible gradient) two by two using the Spearman rank correlation (Spearman 1904). Spearman correlation does not require that KBOs and Centaur color distributions are Gaussian. It is distribution-free and is able to provide meaningful significance levels even for small samples of objects. The method also takes into account the error bars of the measurements. We will discuss results with a correlation coefficient ρ greater than $\sim$0.60 in absolute value. The significance level associated with the correlation coefficient ρ gives the level of evidence against the null hypothesis H_0 which is: *the two samples are not correlated*. Based on the conventions of Efron & Tibshirani (2003) we will interpret the results as: (1) $SL > 95\%$: reasonably strong evidence against H_0, (2) $SL > 97.5\%$: strong evidence against H_0, (3) $SL > 99.7\%$: very strong evidence against H_0 (canonical 3σ Gaussian probability).

Table 5 shows a qualitative summary of the results for all dynamical types and significance levels . The corresponding correlation coefficients and significance levels are listed in Table 6. In this section we discuss only the most relevant results.

6.1.1. The Centaurs

[**Figure 2**]

Results at the 3σ significance level (SL): There is a strong correlation between $B-V$ and $V-J$ indexes (see top of Table 6). The two indexes are thus related by a monotonic function (which is not necessary linear). On Figure 2–a, the data points follow rather well the "reddening curve" quoted in Section 5.2. This curve might be in turn the monotonic function that relates $B-V$ and $V-J$ indexes. This means that the Centaurs

display a quasi-linear reflectivity spectrum over the V→J range. This result was mentioned in McBride et al. (2003); Delsanti et al. (2004), for both KBOs and Centaurs. Logically, a strong correlation also appears between $V-J$ and the visible spectral gradient Gr.

The $B-V$ index also correlate with $V-H$ and $V-K$, with slightly lower ρ and SL. The relation between indexes looks rather linear (see Fig. 2–b and 2–c). The Centaurs with the redder visible colors have also the redder $V-H$ and $V-K$, with a flattening of the spectral slope in the infrared range (red data-points are located below the "reddening curve"). These correlations indicate that a same process is most probably responsible for the surface color behavior from the visible to the near IR range. Other results on the top part of Table 6 confirm this conclusion.

[**Figure 3**]

Results with SL > 97.5% : The most interesting result is the dependency of $H-K$ to the visible indexes ($B-V, V-R, R-I$ and Gr, see Table 6). Although the correlation coefficient ρ is slightly above 0.60 (the correlation is visually quite broad), an interesting result appears: the far end of the near-infrared reflectivity spectrum ($H-K$ region) is bluer for visually redder objects. This results clearly appears on the $B-V$ vs $H-K$ diagram (Fig. 3–a). The Centaurs that have a $H-K$ color bluer than the Sun (bottom right quadrant) are systematically the reddest objects in the visible range. On normalized reflectivity spectra, these objects have the largest visible gradients along with a negative spectral slope over the H→K (∼1.6–2.2μm) range. This might be a hint for the presence of a solid state absorption band long-ward 1.7μm. Only a proper spectroscopic study can unveil the nature of the chemical component causing this feature. In theory, several ices may produce such a reflectance spectrum in the HK region: water ice (broad absorption band around 2μm), CH_4, NH_3, etc, although the relative depth of the absorption features

is closely related to the quantity of ice present on the surface. Silicates are also known to show some absorptions in the 2μm region. Titan tholins (a synthetic involatile material obtained by irradiation of a gas mixture of N_2 and CH_4, to describe the aerosols on the surface of Titan, Khare et al. 1984; Sagan et al. 1984; Imanaka et al. 2004) have a steep visible spectrum and display a broad depression around 2μm.

The objects in our sample that have $H-K$ colors bluer than the Sun are (by increasing value of $H-K$): (33128) 1998 BU_{48}, (83982) 2002 GO_9, (52925) Cyllarus, (7066) Nessus, (5145) Pholus, (44594) 1999 OX_3, (55576) 2002 GB_{10}, (31824) Elatus. As regards real IR spectroscopic studies, (55576) 2002 GB_{10} and (83982) 2002 GO_9 were observed by Doressoundiram et al. (2005a). Water is unambiguously detected for the latter object. The IR spectrum of (55576) 2002 GB_{10} is more difficult to interpret. The composition model presented suggests the presence of 33% of contaminated water ice at the surface of this object. Several works reported the presence of water ice on Pholus (Cruikshank et al. 1998; Brown 2000). Titan tholins have also been invoked to describe its surface composition. Nessus has never been observed with infrared spectroscopy, nor have the other objects. In turn, this trend points toward the Centaurs that can eventually harbor water on their surface (amongst other possibilities), a hypothesis which could be observationally tested. We checked the orbital parameters of these 8 objects, to see if they share some common characteristics. No pattern was identified.

Results at the SL $>$ 95 % level: are consistent with what has been described above. The $V-J$ vs $H-K$ correlation confirms that the Centaurs with $H-K$ bluer than the Sun have systematically the reddest $V-J$ colors (Table 6).

6.1.2. Classical KBOs and other objects

There are no 3σ level correlations for the classical KBOs colors (Table 6). At the lower $SL > 97.5\%$ level, $V-J$, $V-H$, $V-K$ colors are positively correlated (ρ >0.84). As for Centaurs, this result implies that a same coloring process is acting both on the visible and near IR colors. Correlations at the next level ($SL > 95\%$) are consistent with this result.

We found no significant results (*i.e.* $SL > 95\%$) for the current sample (7 objects) of SDO near-IR colors. As regards the resonant objects (9 objects), we have a correlation between $V-J$ vs. Gr, $B-V$, $R-I$ at significance levels 97.6% and lower (Table 6). Again, this implies that most likely a single coloring agent is acting on the visible to near-IR colors.

6.2. Color-physical parameters correlations

[**Table 7**]

[**Table 8**]

We also tested all combinations of color indexes with physical parameters: the orbital semimajor axis a, inclination i, eccentricity e and energy E (defined as $\sqrt{(e^2 + sin^2 i)}$), perihelion q and aphelion Q, absolute magnitude M(1,1) (computed as M(1,1) = R - 5 $\log(r\Delta)$, with r and Δ being the geo- and helio-centric distances in AU resp.). In our tables and later in the text, M(1,1) is more compactly noted H. In this study, we did not take into account the phase effects: the maximum measured opposition effects are of the order of a few tenths of magnitude and therefore should not dramatically influence correlations. We also tested the possible correlations of H with the orbital parameters. For all dynamical sub-classes, there are no 3σ level correlations. In this section we will briefly mention the other results. Table 7 gives a qualitative overview of the trends, correlation coefficients are given in Table 8.

At the $SL > 97.5\%$ level, Centaur $H - K$ and $J - K$ colors show some hints for a correlation with the aphelion distance Q for resp. 17 and 15 objects (see upper part of Table 8). However, the absolute value of the ρ coefficient is slightly lower than 0.60, which means that the correlation is extremely broad.

[**Figure 4**]

As regards classical KBOs, $V - K$ (7 objects) and $V - H$ (8 objects) indexes show a quite strong correlation with absolute magnitude H (Table 8): intrinsically brighter objects show bluer visible-infrared colors than fainter objects. This result was already noticed for visible colors in Hainaut & Delsanti (2002). Usually, absolute magnitude is used as a hint for the size of the objects. It is related to the product of the square diameter and the albedo of the object. KBO albedos are known for a few bright objects. Without albedo measurements, there is no way to rigorously estimate objects diameters. The alternate solution is to assume an albedo value and derive an estimation of the diameter. Given the range of the currently known visible albedos for classical KBOs (from 4 to 40%, Grundy et al. 2005), the estimated diameter can be wrong by a factor up to 3 depending how far is the chosen value from the real (unknown) value. If we assume a common albedo for all objects of the sample (which is *a priori* not guaranteed), the previous result might be translated as "bigger objects show bluer colors than smaller objects". In the context of the resurfacing model developed by Delsanti et al. (2004), cometary activity produces uniform neutral surfaces by redeposition of neutral-colored sub-orbital dust subsequently to the out-gassing. However, only the biggest objects can retain this dust and being resurfaced. Thus, bigger objects show bluer colors which is consistent with the trend above. However, this hypothesis remain speculative: there is no observational evidence for a surface albedo homogeneity, nor routine cometary activity amongst classical KBOs. From plots on Fig. 4–a and 4–b, these correlations appear to be driven by presence of the two very blue objects,

the outliers 1999 SM_{55} and 1996 TO_{66} mentioned in Section 5.2. When removing these two objects, the correlations decrease drastically in significance level. As a conclusion, this result is interesting enough to be mentioned, but it needs definitively to be monitored with more data points.

Classical KBOs also show a broad correlation between $V - J$ and perihelion distance q for 11 objects (Fig. 4–c). This result, although not extremely significant (Table 8) is consistent with findings for the visible colors (Doressoundiram et al. 2005b) and should be monitored on a growing color sample. The same applies to the various low significance level correlations found with inclination and orbital energy that are consistent with results on visible colors by Trujillo & Brown (2002); Doressoundiram et al. (2002) and Hainaut & Delsanti (2002).

The SDOs near-infrared colors (7 objects) do not show any correlation with the orbital parameters nor absolute magnitude with a SL greater than 90%. The $V - J$ colors of the 9 resonant objects correlate with the semimajor axis at a very marginal level.

6.3. Are Centaur visible/near-IR color distributions bimodal ?

Since the very first KBO photometric studies, a controversy was raised on a possible bimodal structure of the visible color distributions of the whole KBO and Centaur population. Indeed, Tegler & Romanishin (1998, 2000, 2003) claimed two separate groups of objects from their dataset: one with neutral (solar) colors, the other with very red colors. Peixinho et al. (2003) showed that this structure appears only amongst the Centaur population for some visible colors. They performed a "dip test" (see Section 6.3.2) on a sample of 20 Centaurs, and found a 99.5% confidence level for a bimodal structure of the $B - R$ distribution and 97.7% for the $V - R$ distribution. This result was confirmed when

testing the Tegler and Romanishin samples of Centaurs alone (while the KBO sample from their paper did not show any statistically significant bimodality, as shown by Peixinho et al. 2003). On the other hand, Bauer et al. (2003) found no bimodal structure in their dataset of 24 Centaurs. However, their work sampled VRI colors, whereas the bimodal structure is found by Peixinho *et al.* to appear most strongly in the $B-R$ index. In this work, we investigate the structure of the near-IR color distributions of Centaurs on a sample of up to 17 objects (JHK colors). We also monitor the structure of the corresponding BVRI colors. We use two statistical tools: the Kolmogorov-Smirnoff test and the "dip test".

6.3.1. The Kolmogorov-Smirnov test

The $J-H$ vs $H-K$ color-color diagram visually displays no obvious bimodal structure (see Fig. 1–b). To quantify this, we use the Kolmogorov-Smirnov (KS) method to test the color distribution structure. We compare the observed 1D color distributions to very simple models of bimodal and unimodal color distributions. The KS test (Kolmogorov 1933) estimates the maximum vertical distance d between the Cumulative Probability Functions of two 1D distributions. This distance d is converted into $Prob$, the probability of the two distributions to be drawn from a same parent distribution. Low values of $Prob$ (*e.g.* a few percent) indicate that the two distributions are statistically incompatible. Large values only indicate that the two distributions are *not* statistically incompatible, but in no case prove that the distributions are drawn from the same parent distribution. We therefore compared some of the observed 1D distributions (resp. $V-J$, ,$J-H$, $H-K$, $J-K$ but also the visible colors for reference) with a simple model of continuous and bimodal distributions (see Fig. 5–a for index $V-J$), that were adjusted to the data to maximize $Prob$. The details on how the different 1D continuous and bimodal synthetic best-fitting distributions are built are described in Hainaut & Delsanti (2002).

[**Figure 5**]

[**Figure 6**]

[**Table 9**]

Table 9 lists the corresponding results: distance d and probability $Prob$. For bimodal model distributions, F is the fraction of objects contained in the "bluer" group. $V-J$ (10 objects), $J-H$ and $J-K$ (15 objects), $H-K$ (17 objects) color distributions show no statistically significant evidence for a bimodal structure. The $H-K$ distribution shows some significant evidence ($Prob > 99.99\%$) for a continuous structure. We also tested the visible color distributions of this present sample. We found that the $B-R$ index show a statistically significant evidence for a bimodal structure with $Prob > 99.9\%$, (see histogram on Fig. 6 and the cumulative probability function on Fig. 5–b). This is compatible with the result reported in Peixinho et al. (2003) on different data. More precisely, the present data sample contains 16 objects in common with Peixinho et al. (with BVR colors compiled from both a larger and more recent set of papers) plus (32532) Thereus.

We also used the 2D version of the KS test (Peacock 1983; Fasano & Franceschini 1987) to probe the structure of some of the color-color diagrams. For example, the $B-V$ vs $H-K$ and $B-R$ vs $H-K$ diagrams (Fig. 3) visually display a bimodal structure. This result is not statistically significant (Table 9), although in the $B-R$ vs $H-K$ space, the bimodal case reaches a significance level of up to 96.4%. All the results are listed in Table 9. No value of $Prob$ lies below a few percent, which means that the observed 2D distributions tested are not statistically incompatible with a continuous or bimodal distribution.

6.3.2. The dip test

[**Table 10**]

This test was designed by Hartigan & Hartigan (1985) to unveil the presence of more than one group in a distribution. The dip statistics is the maximum difference between the studied distribution and the unimodal synthetic distribution that minimizes that maximum difference. In turn, this test is very similar to the KS test used above, except that the dip test finds itself the unimodal distribution by a best-fitting algorithm (whereas in the KS test, the user has to find this best-fitting distribution). The *dip* quantity is close to zero for samples that are drawn from a unimodal distribution. The probability that the computed *dip* is not obtained by chance is available in tables by Hartigan & Hartigan (1985). The results of the dip test for our sample are displayed in Table 10. They confirm the results obtained with the KS test: the JHK colors show no statistical evidence for a bimodal structure.

As regards the visible indexes, the dip test reveals bimodality for $B-V$ with SL=99.5% (more than 2.5σ). Tests for $B-R$ gives a SL of 97.1% (more than 2σ). The algorithm applied here is exactly the same than in Peixinho et al. (2003). In our case, there is a stronger result for $B-V$ than for $B-R$. It is also interesting to note the differences in results between the KS test and the dip test. The latter is specifically designed to detect a bimodal structure and is therefore more robust for this task than the KS test: its results should be regarded as the most conservative. This indicates that the Centaur $B-V$ and $B-R$ bimodality is not a closed subject yet, deserving a more thorough study (that is far beyond the scope of the present work).

7. Summary

We used the 8m-VLT telescope at Cerro Paranal (Chile) and the ISAAC instrument to perform near-IR JHK broadband photometry on a sample of 17 KBOs and Centaurs. We compiled visible-infrared colors (VJHK) from both the published literature and this present

paper for a total of 51 objects. Two outliers (24835) 1995 SM_{55} and (19308) 1996 TO_{66} display peculiar near-IR colors. Both objects were reported to have non-repeatable visible light-curves over time. We performed several statistical tests on the sample of 51 visible-infrared colors to study:

1. the color-color correlations
2. the color-physical parameters (*i.e.* orbital parameters and absolute magnitude) dependences
3. the structure of Centaur color distributions (*e.g.* continuous or bimodal)

Centaurs show some 3σ level color-color correlations that are consistent with the presence of a coloring process that would be acting on surface colors over the visible to near-IR range (0.4 to 2.5μm). Results also show that the Centaurs have a quasi-linear reflectivity spectrum over the V→J spectral range (as previously reported in McBride et al. 2003; Delsanti et al. 2004). The $H-K$ index (17 objects) correlates with the visible colors and spectral gradient (2.5σ level): the optically reddest Centaurs show $H-K$ colors that are systematically bluer than the Sun (as illustrated in Figure 3). The surface of these objects with a negative spectral slope in the H→K range might harbor some chemical components that sign around 1.7–2.2μm (ices such as for H_2O, CH_4, NH_3, etc, silicates or complex organic materials such as Titan tholins). Only a proper near-IR spectroscopic study can unveil the nature of these absorptions. Amongst the 8 objects with $H-K$ colors bluer than the Sun, 3 have been measured with near-IR spectroscopy. Water ice was detected on their surface (evidenced by a broad feature around 2 μm).

Centaurs show no statistically significant bimodal structure in their near-infrared (JHK) color distributions (samples of 15 to 17 objects), as tested with the Kolmogorov-Smirnoff and "dip test" tools (see Tab. 9 and 10). The $B-R$ color distribution of this studied

sample shows some statistically significant evidence for a bimodal structure, which is compatible with results from Peixinho et al. (2003) on different data.

Classical objects show no 3σ level correlations. However, at a lower SL, results are consistent (as for Centaurs) with a coloring process affecting the surfaces from the visible to the near-IR range. The $V - J$ index is correlated with perihelion distance q: objects with a shorter perihelion distance show bluer colors. The same trend was reported by Doressoundiram et al. (2005b) for the $B - R$ colors. We consider this result as interesting (see Fig. 4–c) but yet marginal (11 objects, a correlation coefficient of 0.67 for a SL of 97.6%) and would recommend to monitor this trend with a growing color sample.

Resonant and scattered disk objects are under represented with respect to classical KBOs or Centaurs. Scattered disk objects (7 objects only) show strictly no results with SL>90%. Resonant objects show a marginal dependence of $V - J$ vs. semimajor axis a that should be confirmed on a bigger sample.

8. Acknowledgments

First author thanks C. de Bergh for valuable comments and I. Belskaya for sharing unpublished results. A. Delsanti acknowledges support from the NASA Astrobiology Institute under Cooperative Agreement NNA04CC08A at the Institute for Astronomy (University of Hawaii-Manoa). N. Peixinho acknowledges funding from the Portuguese Foundation for Science and Technology (FCT-SFRH:BD/1094/2000).

Facilities: VLT:Antu (ISAAC)

REFERENCES

Barucci, A., Doressoundiram, A., & Cruikshank, D. 2004, in Comets II, 647

Barucci, M. A. et al. 2002, Astron. Astrophys., 392, 335

Barucci, M. A., Doressoundiram, A., Tholen, D., Fulchignoni, M., & Lazzarin, M. 1999, Icarus, 142, 476

Barucci, M. A., Lazzarin, M., & Tozzi, G. P. 1999, AJ, 117, 1929

Bauer, J., Meech, K., Fernandez, Y., Pittichova, J., Delsanti, A., Boehnhardt, H., & Hainaut, . 2003, Icarus, 166, 195

Boehnhardt, H. et al. 2002, A&A, 395, 297

Boehnhardt, H. et al. 2001, Astron. Astrophys., 378, 653

Brown, M. E. 2000, Astrophys. J., 119, 977

Brown, M. E., & Koresko, C. C. 1998, Astrophys. J., Lett., 505, L65

Brown, R. H., Cruikshank, D. P., & Pendleton, Y. 1999, Astrophys. J., Lett., 519, L101

Chiang, E. I. et al. 2003, Astrophys. J., 126, 430

Cruikshank, D. P. et al. 1998, Icarus, 135, 389

Davies, J. 2000, in Minor Bodies in the Outer Solar System, ed. J. Fitzsimmons & W. (Ed.) (Springer), 9–24

Davies, J. K., Green, S., McBride, N., Muzzerall, E., Tholen, D. J., Whiteley, R. J., Foster, M. J., & Hillier, J. K. 2000, Icarus, 146, 253

Davies, J. K., McBride, N., Ellison, S. L., Green, S. F., & Ballantyne, D. R. 1998, Icarus, 134, 213

Davies, J. K., Sykes, M. V., & Cruikshank, D. P. 1993, Icarus, 102, 166

Delsanti, A., Hainaut, O., Jourdeuil, E., Meech, K., Boehnhardt, H., & Barrera, L. 2004, Astron. Astrophys., 417, 1145

Doressoundiram, A., Barucci, M. A., Tozzi, G., Poulet, F., Boehnhardt, H., de Bergh, C., & Peixinho, N. 2005a, Planet. Space Sci., In Press

Doressoundiram, A., Peixinho, N., de Bergh, C., Fornasier, S., Thébault, P., Barucci, M. A., & Veillet, C. 2002, Astron. J., 124, 2279

Doressoundiram, A., Peixinho, N., Doucet, C., Mousis, O., Barucci, M. A., Petit, J. M., & Veillet, C. 2005b, Icarus, 174, 90

Doressoundiram, A., Tozzi, G. P., Barucci, M. A., Boehnhardt, H., Fornasier, S., & Romon, J. 2003, Astrophys. J., 125, 2721

Dotto, E., Barucci, M. A., Boehnhardt, H., Romon, J., Doressoundiram, A., Peixinho, N., de Bergh, C., & Lazzarin, M. 2003, Icarus, 162, 408

Duncan, M. J., Levison, H. F., & Budd, S. M. 1995, Astrophys. J., 110, 3073

Efron, B., & Tibshirani, R. 2003, An Introduction to the Bootstrap (Chapman & Hall/CRC)

Fasano, G., & Franceschini, A. 1987, Monthly Notices of the Royal Astronomical Society, 225, 155

Fornasier, S. et al. 2004, Astron. Astrophys., 421, 353

Gladman, B., Holman, M., Grav, T., Kavelaars, J., Nicholson, P., Aksnes, K., & Petit, J.-M. 2002, Icarus, 157, 269

Green, S. F., McBride, N., O Ceallaigh, D. P., Fitzsimmons, A., Williams, I. P., & Irwin, M. J. 1997, Mon. Not. R. Astron. Soc., 290, 186

Grundy, W. M., Noll, K. S., & Stephens, D. C. 2005, Icarus, 176, 184

Hainaut, O. R., Delahodde, C. E., Boehnhardt, H., Dotto, E., Barucci K. J. Meech, M. A., Bauer, J. M., West, R. M., & Doressoundiram, A. 2000, Astron. Astrophys., 356, 1076

Hainaut, O. R., & Delsanti, A. C. 2002, Astron. Astrophys., 389, 641

Hardorp, J. 1980, Astron. Astrophys., 88, 334

Hartigan, J., & Hartigan, P. 1985, Ann. Stat., 13, 70

Hartmann, W. K., Cruikshank, D. P., & Degewij, J. 1982, Icarus, 52, 377

Hartmann, W. K., Cruikshank, D. P., Degewij, J., & Capps, R. W. 1981, Icarus, 47, 333

Imanaka, H. et al. 2004, Icarus, 168, 344

Jewitt, D., & Luu, J. 1993, Nature, 362, 730

—. 1998, Astron. J., 115, 1667

Khare, B. N., Sagan, C., Arakawa, E. T., Suits, F., Callcott, T. A., & Williams, M. W. 1984, Icarus, 60, 127

Kolmogorov, A. 1933, Giornale deli Instituto Italiano degli Attuari, 4, 83

Lazzarin, M., Barucci, M. A., Boehnhardt, H., Tozzi, G. P., de Bergh, C., & Dotto, E. 2003, Astrophys. J., 125, 1554

Luu, J., & Jewitt, D. 1996, Astron. J., 112, 2310

McBride, N., Davies, J., Green, S., & Foster, M. 1999, Mon. Not. R. Astron. Soc., 306, 799

McBride, N., Green, S. F., Davies, J. K., Tholen, D. J., Sheppard, S. S., Whiteley, R. J., & Hillier, J. K. 2003, Icarus, 161, 501

Peacock, J. 1983, Monthly Notices of the Royal Astronomical Society, 202, 615

Peixinho, N., Boehnhardt, H., Belskaya, I., Doressoundiram, A., Barucci, M., & Delsanti, A. 2004, Icarus, 170, 153

Peixinho, N., Doressoundiram, A., Delsanti, A., Boehnhardt, H., Barucci, M., & Belskaya, I. 2003, Astron. Astrophys., 410, L29

Persson, S. E., Murphy, D. C., Krzeminski, W., Roth, M., & Rieke, M. J. 1998, Astrophys. J., 116, 2475

Romon-Martin, J., Barucci, M. A., de Bergh, C., Doressoundiram, A., Peixinho, N., & Poulet, F. 2002, Icarus, 160, 59

Sagan, C., Khare, B. N., Thompson, W. R., Murray, B. G. J. P. T., & Squyres, S. W. 1984, BAAS, 16, 668

Sekiguchi, T., Boehnhardt, H., Hainaut, O. R., & Delahodde, C. E. 2002, Astron. Astrophys., 385, 281

Sheppard, S. S., & Jewitt, D. C. 2003, Earth Moon and Planets, 92, 207

Spearman, C. 1904, Am. J. Psychol., 52, 72

Tegler, S., & Romanishin, W. 1998, Nature, 392, 49

—. 2000, Nature, 407, 979

—. 2003, Icarus, 161, 181

Trujillo, C. A., & Brown, M. E. 2002, Astrophys. J., 566, L125

Weintraub, D. A., Tegler, S. C., & Romanishin, W. 1997, Icarus, 128, 456

This manuscript was prepared with the AAS LaTeX macros v5.2.

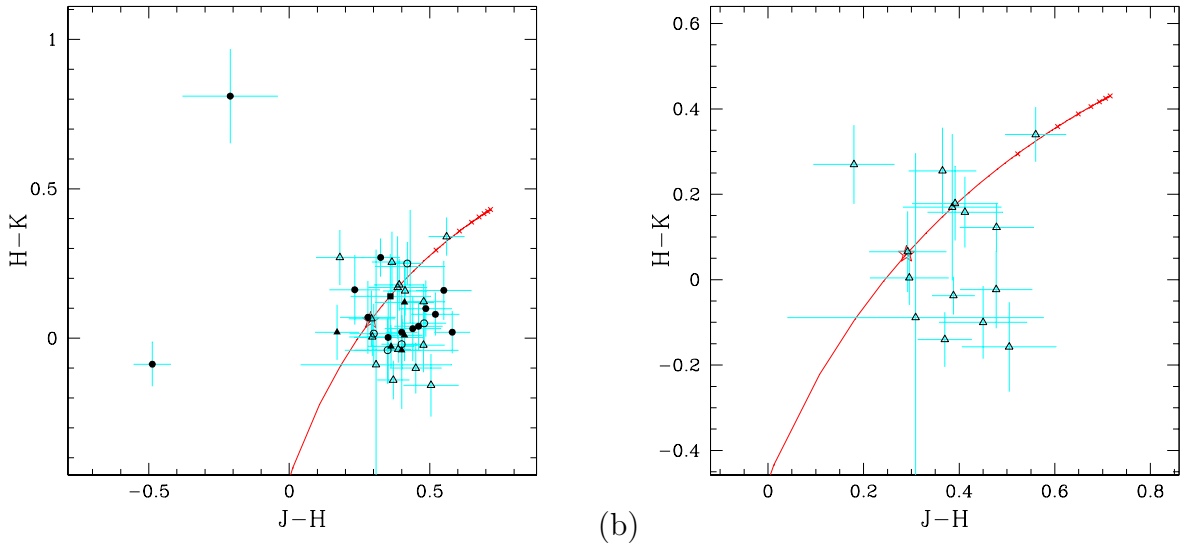

Fig. 1.— $J-H$ *vs* $H-K$ colors. Symbols are: resonant objects (filled triangles), classical objects (filled circles), centaurs (open triangle), scattered disk objects (open circle), sun (open star). The curve is the locus of object with a linear reflectivity spectrum over the J to K range (see Sec. 5.2). On the first plot, top left point is object (19308) 1996 TO_{66}, bottom left point is (24835) 1995 SM_{55}. The second plot shows a close up on Centaur colors only.

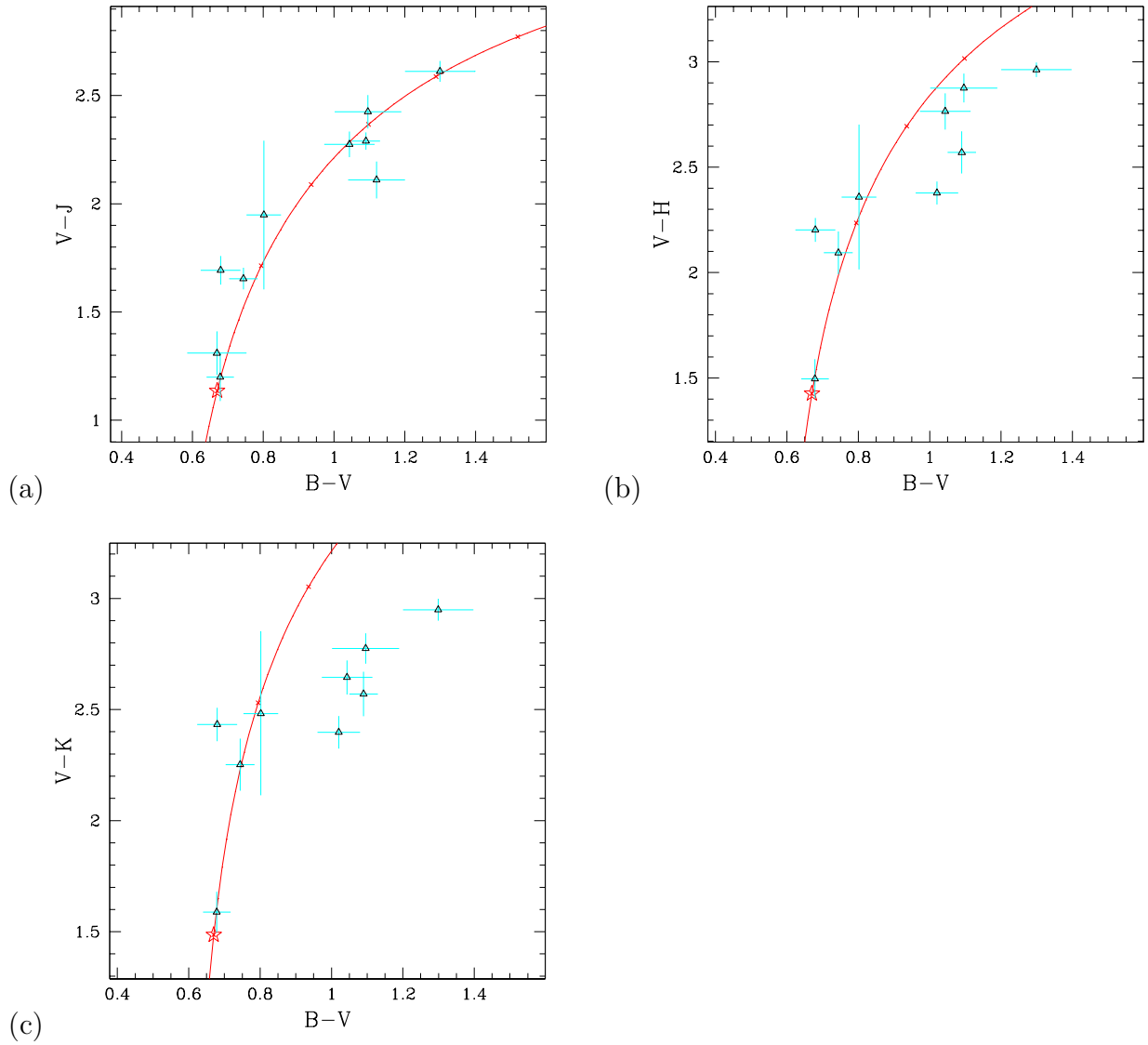

Fig. 2.— Visible/near-IR colors of Centaurs. Solar colors are marked with a star, the curve is the "reddening curve", the locus of objects with a linear reflectivity spectrum.

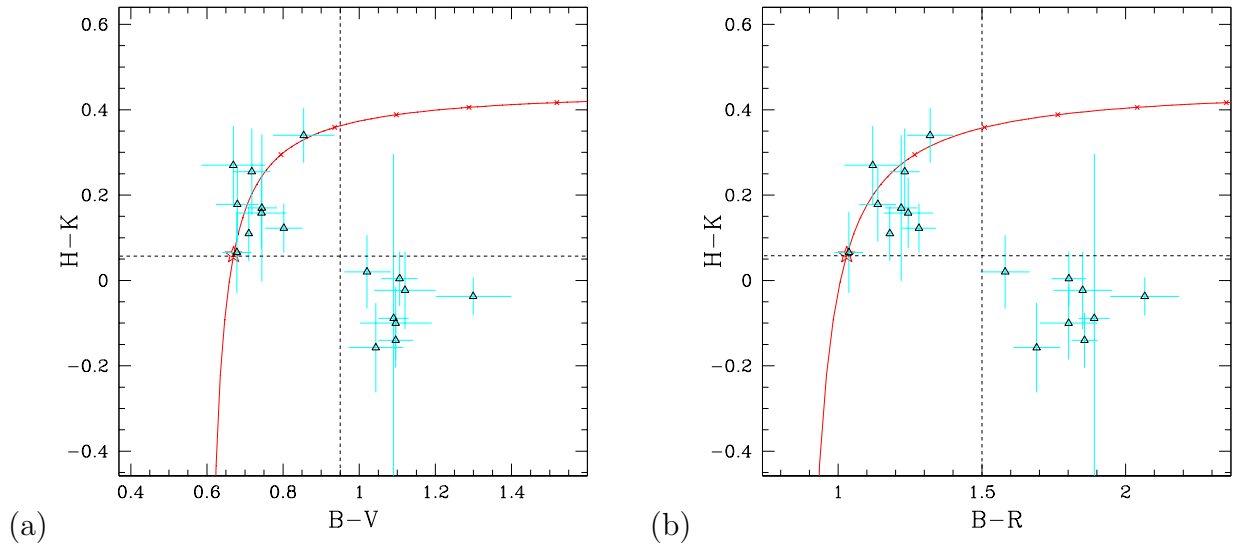

Fig. 3.— $B-V$ vs $H-K$ and $B-R$ vs $H-K$ color diagrams for Centaurs. Conventions are the same than Fig. 1. Horizontal dashed line show the solar $H-K$ value. Vertical dashed line is arbitrarily set to guide the eye.

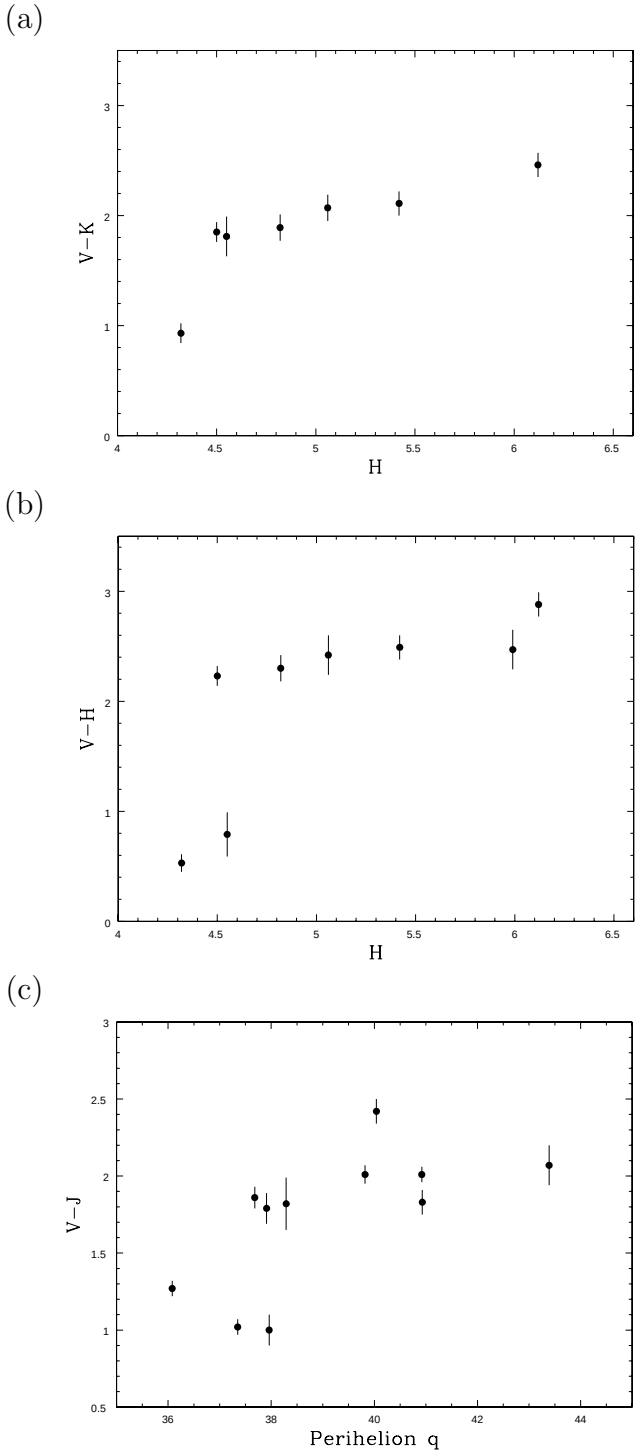

Fig. 4.— Color vs.absolute magnitude and color vs. perihelion distance trends for visible near-IR colors of classical objects.

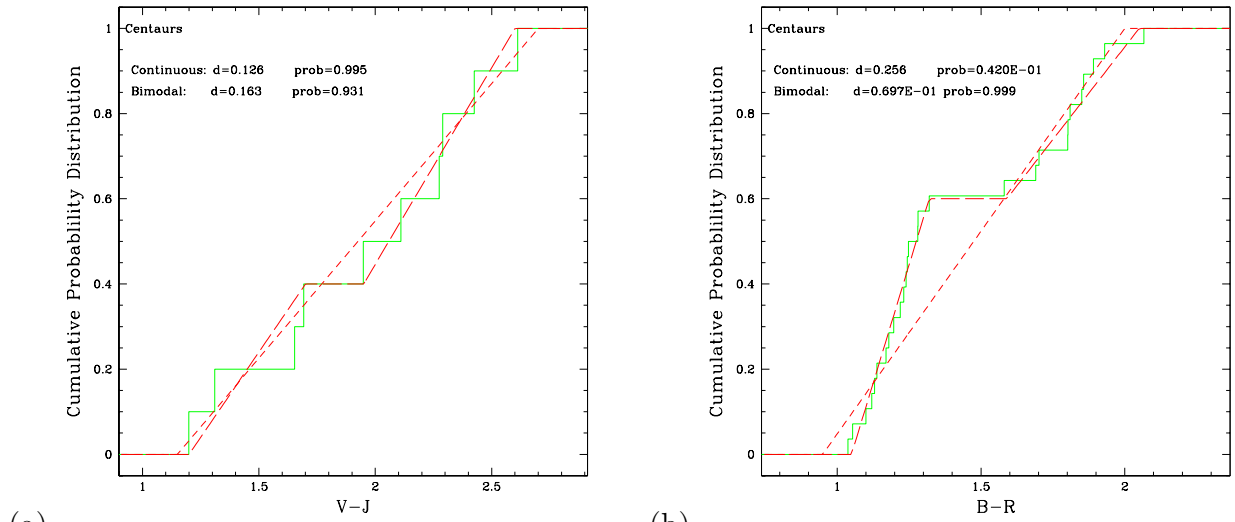

Fig. 5.— Cumulative probability functions of the Centaur $V - J$ colors compared to a continuous and a bimodal (case of F=0.40) model distribution that maximizes the Kolmogorov-Smirnov statistics *Prob* (Graphic a). The same is shown for the visible $B - R$ color distribution (Graphic b).

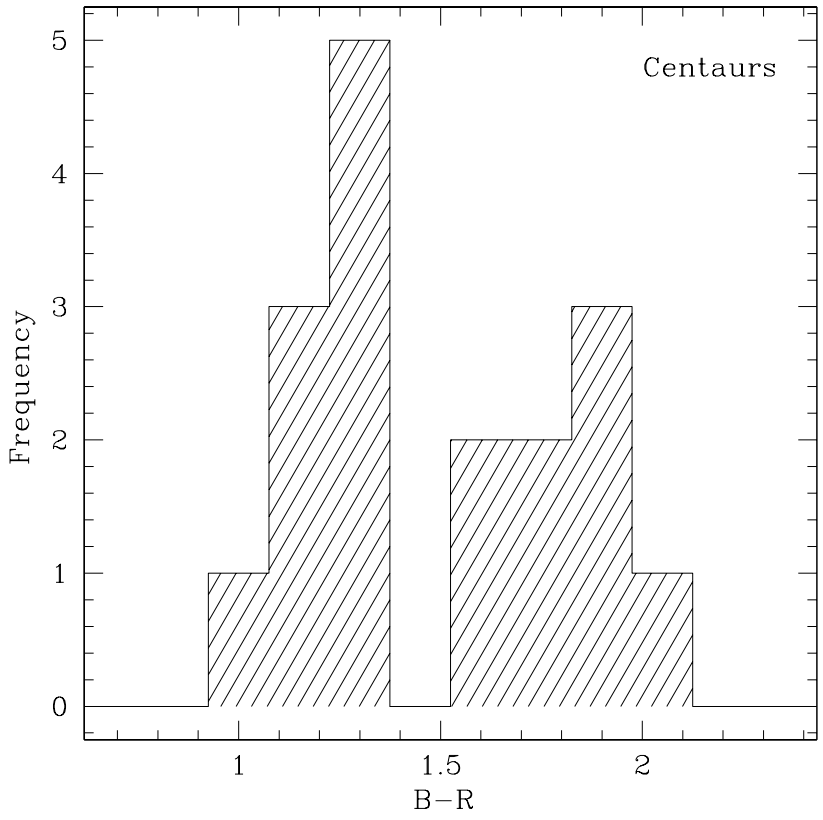

Fig. 6.— Histogram of the B-R colors for the 17 Centaurs studied in this work.

Table 1. Observation circumstances

Object		Type[a]	UT date	r (AU)	Δ (AU)	α^o
	1999 CD_{158}	Cla.	2002-01-21	48.22	47.23	0.0
	2000 OJ_{67}	Cla.	2001-11-12	42.59	42.56	1.3
	2000 PE_{30}	SDO	2001-10-11	37.09	36.79	1.5
	2001 CZ_{31}	Cla.	2001-04-14	41.39	41.07	1.3
	2001 QF_{298}	3:2	2002-08-15	42.62	41.72	0.6
(10370)	Hylonome	Cen.	2002-02-13	19.46	19.20	2.8
(15820)	1994 TB	3:2	2001-08-16	29.35	28.64	1.4
(26181)	1996 GQ_{21}	SDO	2001-05-09	39.28	38.32	0.4
(26375)	1999 DE_9	SDO	2001-05-09	34.00	33.79	1.6
(33128)	1998 BU_{48}	Cen.	2001-04-11	27.66	27.17	1.8
(33340)	1998 VG_{44}	3:2	2001-09-18	30.20	29.82	1.8
(40314)	1999 KR_{16}	SDO.	2001-04-21	37.81	36.81	0.1
(44594)	1999 OX_3	Cen.	2002-08-15	26.29	25.31	0.5
(52872)	Okyrhoe	Cen.	2002-08-16	8.76	8.60	6.5
(60558)	2000 EC_{98}	Cen.	2002-01-15	14.94	14.49	3.4
(66652)	1999 RZ_{253}	Cla.	2002-08-16	41.02	40.01	0.2
(79360)	1997 CS_{29}	Cla.	2001-11-19	43.58	43.14	1.2

[a]Dynamical types of objects are: classical (Cla.), resonant (3:2), scattered disk object (SDO), centaur (Cen.)

Table 2. Photometric measurements

Object	UT date	Time[a]	F[b]	Magnitude	Object	UT date	Time	F	Magnitude
1999 CD_{158}	2002-01-21	05:10	H	19.99 ± 0.07	(33128) 1998 BU_{48}	2001-04-11	23:45	J	19.86 ± 0.08
	2002-01-21	05:57	H	20.05 ± 0.07		2001-04-11	00:02	H	19.51 ± 0.06
	2002-01-21	06:29	J	20.45 ± 0.06		2001-04-11	00:59	J	20.03 ± 0.08
	2002-01-21	06:47	K	19.94 ± 0.06		2001-04-11	01:15	K	19.70 ± 0.07
2000 OJ_{67}	2001-11-12	00:04	H	20.74 ± 0.07	(33340) 1998 VG_{44}	2001-09-18	07:24	J	20.03 ± 0.06
	2001-11-12	01:02	J	21.01 ± 0.06		2001-09-18	07:36	H	19.58 ± 0.05
	2001-11-12	01:17	K	20.67 ± 0.12		2001-09-18	08:28	J	19.99 ± 0.06
	2001-11-12	01:57	J	21.04 ± 0.07		2001-09-18	08:41	K	19.57 ± 0.06
	2001-11-12	02:11	K	20.61 ± 0.12					
					(40314) 1999 KR_{16}	2001-04-21	04:08	J	19.56 ± 0.05
2000 PE_{30}	2001-10-11	01:13	H	20.34 ± 0.04		2001-04-21	04:20	H	18.96 ± 0.05
	2001-10-11	02:11	J	20.78 ± 0.04		2001-04-21	05:04	J	19.52 ± 0.05
	2001-10-11	02:26	K	20.08 ± 0.06		2001-04-21	05:16	K	18.94 ± 0.05
	2001-10-11	03:06	J	20.75 ± 0.04					
	2001-10-11	03:18	K	20.11 ± 0.06	(44594) 1999 OX_3	2002-08-15	00:00	H	19.19 ± 0.04
						2002-08-15	00:20	K	19.19 ± 0.07
2001 CZ_{31}	2001-04-14	00:15	J	20.82 ± 0.07		2002-08-15	00:35	J	19.63 ± 0.04
	2001-04-14	00:19	H	20.27 ± 0.07		2002-08-16	00:10	H	19.15 ± 0.06
	2001-04-14	00:32	K	20.11 ± 0.07		2002-08-16	00:30	K	19.20 ± 0.07
						2002-08-16	00:50	J	19.67 ± 0.04
2001 QF_{298}	2002-08-15	03:10	J	20.27 ± 0.06					
	2002-08-15	03:20	H	20.04 ± 0.06	(52872) Okyrhoe	2002-08-16	06:10	J	19.04 ± 0.03
	2002-08-15	03:40	K	19.84 ± 0.07		2002-08-16	06:20	H	18.54 ± 0.05
	2002-08-15	03:54	J	20.23 ± 0.05		2002-08-16	06:40	K	18.41 ± 0.05
	2002-08-15	09:30	J	20.21 ± 0.05		2002-08-16	07:00	J	19.09 ± 0.03
	2002-08-15	09:40	H	19.99 ± 0.08		2002-08-16	08:45	J	19.05 ± 0.03
	2002-08-15	10:00	K	19.87 ± 0.09		2002-08-16	08:55	H	18.68 ± 0.05
	2002-08-16	10:05	J	20.21 ± 0.05		2002-08-16	09:15	K	18.49 ± 0.06
						2002-08-16	09:30	J	19.13 ± 0.03
(10370) Hylonome	2002-02-13	07:31	H	20.66 ± 0.06					
	2002-02-13	07:59	J	20.84 ± 0.06	(60558) 2000 EC_{98}	2002-01-16	07:45	H	19.91 ± 0.05

Table 2—Continued

Object	UT date	Time[a]	F[b]	Magnitude	Object	UT date	Time	F	Magnitude
	2002-02-13	08:06	K	20.39 ± 0.07		2002-01-16	08:14	J	20.48 ± 0.06
	2002-02-13	09:01	J	20.95 ± 0.05		2002-01-16	08:21	K	19.57 ± 0.04
						2002-01-16	09:20	J	20.45 ± 0.05
(15820) 1994 TB	2001-08-16	06:48	J	20.57 ± 0.06					
	2001-08-16	07:06	H	20.19 ± 0.06	(66652) 1999 RZ_{253}	2002-08-16	07:10	J	20.08 ± 0.05
	2001-08-16	08:07	J	20.62 ± 0.08		2002-08-16	07:30	H	19.59 ± 0.08
						2002-08-16	08:00	K	19.49 ± 0.05
(26181) 1996 GQ_{21}	2001-05-09	02:43	J	18.72 ± 0.07		2002-08-16	08:30	J	20.02 ± 0.05
	2001-05-09	02:48	H	18.24 ± 0.06					
	2001-05-09	03:14	J	18.73 ± 0.07	(79360) 1997 CS_{29}	2001-11-19	07:23	H	19.74 ± 0.06
	2001-05-09	03:19	K	18.19 ± 0.06		2001-11-19	07:52	J	20.11 ± 0.06
						2001-11-19	07:58	K	19.70 ± 0.06
(26375) 1999 DE_9	2001-05-09	01:51	J	18.78 ± 0.08		2001-11-19	08:55	J	20.13 ± 0.06
	2001-05-09	01:54	H	18.46 ± 0.08					
	2001-05-09	02:08	K	18.50 ± 0.08					

[a]UT times are mid-exposure

[b]Filter name

Table 3. ESO Large Program near-IR colors

Object	J-H $\pm\sigma$	H-K $\pm\sigma$	J-K $\pm\sigma$	Reference
Solar colors	0.23	0.06	0.29	Hardorp (1980); Hartmann et al. (1982)
1999 CD_{158}	0.43 ± 0.09†	0.08 ± 0.09†	0.51 ± 0.08	This paper
2000 OJ_{67}	0.28 ± 0.09*	0.07 ± 0.12	0.35 ± 0.12*	···
2000 PE_{30}	0.42 ± 0.05*	0.25 ± 0.07‡	0.67 ± 0.07*,‡	···
2001 CZ_{31}	0.55 ± 0.09	0.16 ± 0.09	0.71 ± 0.09	···
2001 QF_{298}	0.23 ± 0.09	0.16 ± 0.11	0.39 ± 0.11	···
(10370) Hylonome	0.18 ± 0.08	0.27 ± 0.09	0.45 ± 0.09	···
(15820) 1994 TB	0.38 ± 0.08	—	—	···
(26181) 1996 GQ_{21}	0.48 ± 0.07*	0.05 ± 0.08	0.53 ± 0.07*	···
(26375) 1999 DE_{9}	0.32 ± 0.11	−0.04 ± 0.11	0.28 ± 0.11	···
(33128) 1998 BU_{48}	0.52 ± 0.10	−0.19 ± 0.09	0.33 ± 0.10	···
(33340) 1998 VG_{44}	0.41 ± 0.06	0.01 ± 0.08	0.42 ± 0.08	···
(40314) 1999 KR_{16}	0.58 ± 0.06*	0.02 ± 0.07	0.60 ± 0.06*	···
(44594) 1999 OX_{3}	0.48 ± 0.07	−0.02 ± 0.09	0.46 ± 0.08	···
(52872) Okyrhoe	0.43 ± 0.09	0.16 ± 0.08	0.60 ± 0.07	···
(60558) 2000 EC_{98}	0.56 ± 0.06*	0.34 ± 0.06‡	0.90 ± 0.05*,‡	···
(66652) 1999 RZ_{253}	0.49 ± 0.09	0.10 ± 0.09	0.58 ± 0.06	···
(79360) 1997 CS_{29}	0.38 ± 0.08*	0.04 ± 0.08	0.42 ± 0.08*	···
(26181) 1996 GQ_{21}	—	—	0.77 ± 0.06	Doressoundiram et al. (2003)
(26375) 1999 DE_{9}	0.29 ± 0.06	0.07 ± 0.06	0.36 ± 0.06	Doressoundiram et al. (2003)
(32532) Thereus	0.51 ± 0.04	0.11 ± 0.06	0.62 ± 0.06	Barucci et al. (2002)
(47171) 1999 TC_{36}	0.36 ± 0.06	−0.03 ± 0.07	0.33 ± 0.06	Dotto et al. (2003)
(52872) Okyrhoe	0.36 ± 0.05	0.20 ± 0.04	0.56 ± 0.05	Dotto et al. (2003)
(54598) Bienor	0.35 ± 0.06	0.14 ± 0.05	0.49 ± 0.05	Dotto et al. (2003)
(55565) 2002 AW_{97}	0.33 ± 0.04	0.23 ± 0.08	0.56 ± 0.08	Doressoundiram et al. (2005a)
(55576) 2002 GB_{10}	0.29 ± 0.06	−0.08 ± 0.08	0.21 ± 0.06	Doressoundiram et al. (2005a)
(63252) 2001 BL_{41}	0.37 ± 0.05	0.24 ± 0.06	0.61 ± 0.06	Doressoundiram et al. (2003)
(83982) 2002 GO_{9}	0.37 ± 0.06	−0.03 ± 0.07	0.34 ± 0.04	Doressoundiram et al. (2005a)

Note. — Indexes are computed from the magnitudes from table 2 the closest in time, apart from: * computed from the average of the J magnitudes, † from the average of H magnitudes, ‡ from the average of the K magnitudes

available.

Table 4. Compilation of published near-IR colors

Object	Type[a]	$V-J\pm\sigma$	$J-H\pm\sigma$	$H-K\pm\sigma$	$J-K\pm\sigma$	Reference
1995 HM_5	3:2	—	1.20 ± 0.47	—	—	1
1996 TQ_{66}	3:2	2.43 ± 0.12	—	—	—	2
1996 TS_{66}	Cla.	1.82 ± 0.17	0.65 ± 0.07	—	—	2, 3
1999 CD_{158}	Cla.	1.86 ± 0.07	0.44 ± 0.10	0.03 ± 0.10	0.47 ± 0.09	6, this paper
2000 KK_4	Cla.	1.79 ± 0.10	—	—	—	4
2000 OJ_{67}	Cla.	—	0.28 ± 0.09	0.07 ± 0.12	0.35 ± 0.12	this paper
2000 OK_{67}	Cla.	2.42 ± 0.08	0.46 ± 0.08	0.04 ± 0.07	0.50 ± 0.09	6
2000 PE_{30}	SDO	—	0.42 ± 0.05	0.25 ± 0.07	0.67 ± 0.07	this paper
2001 CZ_{31}	Cla.	—	0.55 ± 0.09	0.16 ± 0.09	0.71 ± 0.09	this paper
2001 QF_{298}	3:2	—	0.23 ± 0.09	0.16 ± 0.11	0.39 ± 0.11	this paper
(02060) Chiron	Cen.	1.20 ± 0.11	0.29 ± 0.08	0.06 ± 0.09	0.36 ± 0.08	7, 8, 9
(05145) Pholus	Cen.	2.61 ± 0.04	0.39 ± 0.04	−0.04 ± 0.04	0.35 ± 0.04	8, 9, 10, 11
(07066) Nessus	Cen.	2.29 ± 0.04	0.31 ± 0.26	−0.08 ± 0.38	0.31 ± 0.28	8, 9
(08405) Asbolus	Cen.	1.65 ± 0.04	0.39 ± 0.10	0.17 ± 0.17	0.59 ± 0.14	8, 9, 11, 12
(10199) Chariklo	Cen.	1.95 ± 0.34	0.48 ± 0.07	0.12 ± 0.05	0.56 ± 0.07	8, 9, 13
(10370) Hylonome	Cen.	1.31 ± 0.10	0.18 ± 0.08	0.27 ± 0.09	0.45 ± 0.09	8, this paper
(15789) 1993 SC	3:2	2.43 ± 0.15	0.40 ± 0.20	−0.04 ± 0.19	0.36 ± 0.08	2, 3
(15820) 1994 TB	3:2	2.37 ± 0.16	0.41 ± 0.10	0.12 ± 0.12	0.57 ± 0.12	2, 6, this paper
(15874) 1996 TL_{66}	SDO	1.45 ± 0.11	0.35 ± 0.11	−0.04 ± 0.11	0.31 ± 0.07	2, 3
(15875) 1996 TP_{66}	3:2	2.31 ± 0.06	0.17 ± 0.07	0.02 ± 0.09	0.19 ± 0.08	2, 3
(19308) 1996 TO_{66}	Cla.	1.00 ± 0.10	−0.21 ± 0.17	0.81 ± 0.15	0.60 ± 0.09	2, 3
(19521) Chaos	Cla.	1.83 ± 0.08	0.40 ± 0.05	0.02 ± 0.05	0.42 ± 0.05	2, 6
(20000) Varuna	Cla.	2.01 ± 0.05	—	—	—	4
(24835) 1995 SM_{55}	Cla.	1.02 ± 0.05	−0.49 ± 0.06	−0.09 ± 0.07	−0.57 ± 0.07	4, 6
(26181) 1996 GQ_{21}	SDO	2.44 ± 0.06	0.48 ± 0.07	0.05 ± 0.08	0.68 ± 0.11	4, 15, this paper
(26308) 1998 SM_{165}	2:1	2.37 ± 0.06	0.52 ± 0.08	0.08 ± 0.07	0.60 ± 0.08	4, 6
(26375) 1999 DE_9	SDO	1.89 ± 0.06	0.30 ± 0.08	0.01 ± 0.10	0.32 ± 0.09	4, 15, this paper
(29981) 1999 TD_{10}	SDO	1.79 ± 0.05	—	—	—	4
(31824) Elatus	Cen.	—	—	0.02 ± 0.08	—	6
(32532) Thereus	Cen.	—	—	0.11 ± 0.06	—	16
(32929) 1995 QY_9	3:2	2.03 ± 0.20	—	—	—	2
(33128) 1998 BU_{48}	Cen.	2.27 ± 0.05	0.50 ± 0.09	−0.16 ± 0.10	0.35 ± 0.09	6, this paper

Table 4—Continued

Object	Type[a]	$V-J\pm\sigma$	$J-H\pm\sigma$	$H-K\pm\sigma$	$J-K\pm\sigma$	Reference
(33340) 1998 VG_{44}	3:2	—	0.41 ± 0.06	0.01 ± 0.08	0.42 ± 0.08	this paper
(35671) 1998 SN_{165}	Cla.	1.27 ± 0.05	—	—	—	4
(38628) Huya	3:2	1.97 ± 0.05	—	—	—	4
(40314) 1999 KR_{16}	SDO	—	0.58 ± 0.06	0.02 ± 0.07	0.60 ± 0.06	this paper
(44594) 1999 OX_3	Cen.	2.11 ± 0.08	0.48 ± 0.07	−0.02 ± 0.09	0.45 ± 0.08	4, this paper
(47171) 1999 TC_{36}	3:2	2.33 ± 0.06	0.36 ± 0.08	−0.03 ± 0.07	0.36 ± 0.08	4, 6, 14
(47932) 2000 GN_{171}	3:2	1.76 ± 0.06	—	—	—	4
(48639) 1995 TL_8	SDO	2.42 ± 0.05	0.40 ± 0.07	−0.02 ± 0.08	0.38 ± 0.07	6
(52872) Okyrhoe	Cen.	—	0.41 ± 0.07	0.16 ± 0.08	0.58 ± 0.06	14, this paper
(52975) Cyllarus	Cen.	2.42 ± 0.07	0.45 ± 0.09	−0.10 ± 0.08	0.35 ± 0.09	6
(54598) Bienor	Cen.	1.69 ± 0.06	0.39 ± 0.09	0.18 ± 0.08	0.58 ± 0.14	6, 14
(55565) 2002 AW_{197}	Cla.	—	0.32 ± 0.06	0.27 ± 0.06	0.59 ± 0.06	5
(55576) 2002 GB_{10}	Cen.	—	0.30 ± 0.08	0.00 ± 0.06	0.30 ± 0.08	5
(60558) 2000 EC_{98}	Cen.	—	0.56 ± 0.06	0.34 ± 0.06	0.90 ± 0.05	this paper
(63252) 2001 BL_{41}	Cen.	—	0.36 ± 0.07	0.25 ± 0.10	0.62 ± 0.09	15
(66652) 1999 RZ_{253}	Cla.	2.01 ± 0.06	0.48 ± 0.09	0.10 ± 0.09	0.58 ± 0.06	4, this paper
(79360) 1997 CS_{29}	Cla.	2.07 ± 0.13	0.35 ± 0.12	0.00 ± 0.15	0.36 ± 0.16	1, 2, this paper
(83982) 2002 GO_{09}	Cen.	—	0.37 ± 0.05	−0.14 ± 0.06	0.33 ± 0.10	5
(91133) 1998 HK_{151}	3:2	1.57 ± 0.09	—	—	—	4

[a]Types of objects are: classical (Cla.), resonant (3:2, 2:1), scattered disk object (SDO), centaur (Cen.)

References. — 1: Boehnhardt et al. (2001), 2: Davies et al. (2000), 3: Jewitt & Luu (1998) , 4: McBride et al. (2003), 5: Doressoundiram et al. (2005a), 6: Delsanti et al. (2004), 7: Hartmann et al. (1981), 8: Davies (2000), 9: Davies et al. (1998), 10: Davies et al. (1993), 11: Weintraub et al. (1997), 12: Romon-Martin et al. (2002), 13: McBride et al. (1999), 14: Dotto et al. (2003), 15: Doressoundiram et al. (2003), 16: Barucci et al. (2002)

Note. — This is a compilation of colors averaged from different observers. Only colors computed from simultaneous photometry (both filters observed within a couple of hours) are used. Some differences are noticed with Table 3 which reports colors as published by their authors (example: (32532) Thereus).

Table 5. Qualitative summary of color-color correlations

	3σ SL[a] level		$97.50 < SL \leq 99.73$		$95.0 < SL \leq 97.5$	
Type	n[b]	Correlation	n	Correlation	n	Correlation
Centaurs	10	B-V vs. V-J, V-H, V-K	10	V-J, V-H, V-K vs. vis. colors & Gr[c]	10	V-J, V-H vs. H-K
			17	H-K vs. vis. colors & Gr		
Classicals	···	No result	7	V-J vs V-K	11	V-J vs vis. colors & Gr
			8	V-J vs V-H		
			7	V-H vs V-K		
Resonants	···	No result	9	V-J vs. Gr	9	V-J vs B-V, R-I
Scattered disk	···	No result	···	No result	···	No result

[a]significance level of the correlation coefficient

[b]number of objects for this correlation

[c]visible gradient

Note. — Corresponding correlation coefficients are listed in Table 6

Table 6. Color-color correlations

	$SL \geq 99.73$ (3σ level)					$97.50 < SL \leq 99.73$					$95.0 < SL \leq 97.5$			
	n[a]	$\langle\rho\rangle^{+\sigma}_{-\sigma}$[b]	SL[c]	σ_{SL}		n	$\langle\rho\rangle^{+\sigma}_{-\sigma}$	SL	σ_{SL}		n	$\langle\rho\rangle^{+\sigma}_{-\sigma}$	SL	σ_{SL}
CENTAURS														
VJ *vs.* BV	10	$0.88^{+0.05}_{-0.09}$	99.92	3.35	VJ *vs.* VR	10	$0.82^{+0.08}_{-0.13}$	99.64	2.91	VJ *vs.* HK	10	$-0.66^{+0.17}_{-0.12}$	96.08	2.06
VJ *vs.* Gr	10	$0.87^{+0.05}_{-0.09}$	99.90	3.29	VJ *vs.* RI	10	$0.82^{+0.09}_{-0.18}$	99.66	2.92	HK *vs.* VH	10	$-0.67^{+0.18}_{-0.13}$	96.67	2.13
VJ *vs.* VH	10	$0.94^{+0.03}_{-0.06}$	99.99	4.04	VJ *vs.* IJ	9	$0.78^{+0.09}_{-0.15}$	98.69	2.48	BV *vs.* IJ	9	$0.67^{+0.13}_{-0.19}$	95.09	1.97
VJ *vs.* VK	10	$0.91^{+0.04}_{-0.09}$	99.98	3.70										
					HK *vs.* BV	17	$-0.64^{+0.12}_{-0.09}$	99.42	2.76					
VH *vs.* BV	10	$0.86^{+0.06}_{-0.10}$	99.87	3.22	HK *vs.* VR	17	$-0.62^{+0.15}_{-0.11}$	99.15	2.63					
VH *vs.* VK	10	$0.89^{+0.05}_{-0.10}$	99.95	3.48	HK *vs.* RI	17	$-0.59^{+0.18}_{-0.13}$	98.67	2.48					
					HK *vs.* Gr	17	$-0.64^{+0.13}_{-0.10}$	99.40	2.75					
VK *vs.* BV	10	$0.83^{+0.07}_{-0.12}$	99.73	3.00	HK *vs.* JK	15	$0.62^{+0.13}_{-0.18}$	98.72	2.49					
					VH *vs.* VR	10	$0.78^{+0.10}_{-0.16}$	99.15	2.63					
					VH *vs.* RI	10	$0.79^{+0.11}_{-0.20}$	99.37	2.73					
					VH *vs.* IJ	9	$0.81^{+0.09}_{-0.15}$	99.17	2.64					
					VH *vs.* Gr	10	$0.83^{+0.07}_{-0.12}$	99.71	2.98					
					VK *vs.* VR	10	$0.77^{+0.11}_{-0.18}$	99.07	2.60					
					VK *vs.* RI	10	$0.77^{+0.11}_{-0.20}$	99.07	2.60					
					VK *vs.* IJ	9	$0.78^{+0.10}_{-0.16}$	98.72	2.49					
					VK *vs.* Gr	10	$0.82^{+0.09}_{-0.15}$	99.66	2.93					
CLASSICALS														
					VH *vs.* VK	7	$0.91^{+0.05}_{-0.09}$	99.56	2.85	VJ *vs.* Gr	11	$0.65^{+0.11}_{-0.16}$	97.05	2.18
					VJ *vs.* VK	7	$0.90^{+0.05}_{-0.09}$	99.47	2.79	VJ *vs.* VR	11	$0.63^{+0.14}_{-0.19}$	96.38	2.09
					VJ *vs.* VH	8	$0.84^{+0.08}_{-0.16}$	99.17	2.64	VJ *vs.* RI	10	$0.65^{+0.15}_{-0.22}$	95.76	2.03
										JH *vs.* VK	7	$0.76^{+0.12}_{-0.22}$	95.27	1.98
RESONANTS														
					VJ *vs.* Gr	9	$0.74^{+0.12}_{-0.18}$	97.60	2.26	VJ *vs.* BV	9	$0.70^{+0.14}_{-0.23}$	96.37	2.09
										VJ *vs.* RI	9	$0.68^{+0.15}_{-0.23}$	95.64	2.02

[a]Number of objects in the sample studied

[b]Spearman Rank correlation coefficient and 1σ errors

[c]Significance level of ρ

Table 7. Qualitative summary of color-physical parameters correlations

	3σ SL[a] level		$97.50 < SL \leq 99.73$		$95.0 < SL \leq 97.5$	
Type	n[b]	Correlation	n	Correlation	n	Correlation
Centaurs	···	No result	17	H-K vs Q ?	15	J-K vs a ?
			15	J-K vs Q ?		
Classicals	···	No result	8	V-H vs H	8	V-H vs i, E
			7	V-K vs H	7	V-K vs i
			11	V-J vs q	11	V-J vs a, E
Resonants	···	No result	···	No result	9	V-J vs a
Scattered disk	···	No result	···	No result	···	No result

[a]significance level of the correlation coefficient

[b]number of objects for this correlation

Note. — Corresponding correlation coefficients are listed in Table 8

Table 8. Color - physical parameters correlations

		$97.50 < SL \leq 99.73$					$95.0 < SL \leq 97.5$			
Type		n[a]	$\langle\rho\rangle_{-\sigma}^{+\sigma}$[b]	SL[c]	σ_{SL}		n	$\langle\rho\rangle_{-\sigma}^{+\sigma}$	SL	σ_{SL}
Centaurs	HK *vs.* Q	17	$-0.57^{+0.12}_{-0.10}$	98.42	2.41	JK *vs.* a	15	$-0.57^{+0.13}_{-0.11}$	97.28	2.21
	JK *vs.* Q	15	$-0.58^{+0.14}_{-0.11}$	97.65	2.27					
	HK *vs.* a	17	$-0.55^{+0.11}_{-0.09}$	97.82	2.29					
Classicals	VH *vs.* H	8	$0.88^{+0.06}_{-0.13}$	99.61	2.89	VH *vs.* i	8	$-0.77^{+0.12}_{-0.08}$	97.45	2.23
	VK *vs.* H	7	$0.92^{+0.04}_{-0.08}$	99.66	2.93	VK *vs.* i	7	$-0.78^{+0.08}_{-0.06}$	96.21	2.08
	VJ *vs.* q	11	$0.67^{+0.08}_{-0.09}$	97.62	2.26	VH *vs.* E	8	$-0.76^{+0.15}_{-0.10}$	97.04	2.17
						VJ *vs.* E	11	$-0.60^{+0.08}_{-0.07}$	95.08	1.97
						VJ *vs.* a	11	$0.62^{+0.08}_{-0.09}$	95.85	2.04
Resonants						VJ *vs.* a	9	$-0.72^{0.10}_{-0.08}$	97.04	2.17

[a]Number of objects in the sample studied

[b]Spearman Rank correlation coefficient and 1σ errors

[c]Significance level of ρ

Table 9. Centaurs color bimodality: the Kolmogorov-Smirnoff tests

Color	n[a]	Model	F[b]	d	*Prob*(%)
J−H	15	Continuous	—	0.128	95.3
		Bimodal	0.26	0.234	33.9
H−K	17	Continuous	—	0.082	>99.99
		Bimodal	0.48	0.270	14.1
J−K	15	Continuous	—	0.211	46.9
		Bimodal	0.46	0.265	20.6
V−J	10	Continuous	—	0.126	99.5
		Bimodal	0.20	0.164	92.9
		Bimodal	0.40	0.163	93.1
B−V	17	Continuous	—	0.213	13.9
		Bimodal	0.60	0.127	73.1
B−R	17	Continuous	—	0.256	4.2
		Bimodal	0.60	0.069	99.9
V−J *vs.* J−H	10	Continuous	—	0.188	88.0
		Bimodal	0.20	0.213	76.5
V−J *vs.* J−K	10	Continuous	—	0.181	90.5
		Bimodal	0.20	0.256	54.4
J−H *vs.* H−K	15	Continuous	—	0.161	87.9
		Bimodal	0.50	0.254	34.9
B−V *vs.* H−K	17	Continuous	—	0.267	21.6
		Bimodal	0.50	0.131	95.1
B−R *vs.* H−K	17	Continous	—	0.268	21.4
		Bimodal	0.50	0.126	96.4

[a]number of objects in the sample studied

[b]fraction of objects in the first group

Table 10. Dip test results for the Centaurs

Color	n[a]	Dip	SL(%)
J−H	15	0.071	25.0
H−K	17	0.070	32.0
J−K	15	0.112	91.9
V−J	10	0.087	38.3
B−V	17	0.136	99.5
B−R	17	0.121	97.1

[a]Number of objects in the sample studied